EXTENDED NEUTROSPHERIC MODELLING FOR THE GNSS-BASED DETERMINATION OF HIGH-RESOLUTION ATMOSPHERIC WATER VAPOUR FIELDS

Modelamento netrosférico aumentado para a determinação de campos de vapor d'água atmosféricos com base em sinais de alta resolução gnss.

DIPL.-ING. XIAOGUANG LUO
DR.-ING. MICHAEL MAYER
PROF. DR.-ING. DR. H.C. BERNHARD HECK

Geodetic Institute
University Karlsruhe (TH)
Englerstr. 7, D – 76131 Karlsruhe, Germany
E-mail: {luo, mmayer, heck}@gik.uni-karlsruhe.de
Phone: ++ 49 – 7237 – 608-3668

ABSTRACT

Signals of global navigation satellite systems (GNSS) are delayed by propagating through the Earth's electrically neutral atmosphere. This delay term plays an important role in GNSS positioning and has been taken into account in high-precision geodetic applications. The neutrospheric delay can be subdivided into a dry and a complementary wet component. The wet component amounts to typically less than 10% of the total neutrospheric delay and can be used to determine high-resolution atmospheric water vapour fields based on extended neutrospheric modelling. The approach outlined in the present paper combines empirical neutrospheric a priori model, site-specific neutrosphere parameters and residuals of GNSS phase observations. Using so-called single-layer models, the derived atmospheric water vapour fields are two-dimensionally reconstructed and visualised. Applying this extended neutrospheric model to generate water vapour fields within a regional GNSS network, the results indicate that both the temporal and the spatial resolution of the determined water vapour fields are improved in comparison to the conventional neutrospheric modelling.

Keywords: GNSS; Residuals; Neutrospheric Modelling; Atmospheric Water Vapour.

RESUMO

Os sinais oriundos dos sistemas de navegação globais por satélite (GNSS) sofrem um atraso durante sua propagação através da camada eletricamente neutra da atmosfera terrestre. Este atraso tem um papel fundamental no posicionamento GNSS e tem sido levado em conta nas aplicações geodésicas de alta precisão. O atraso neutrosférico pode ser subdividido em uma componente seca e uma componente complementar úmida. A quantidade correspondente a componente úmida é tipicamente inferior a 10% do atraso total, e pode ser utilizada na determinação de campos de vapor d'água atmosférico de alta resolução baseados no modelo aumentado da neutrosfera. A abordagem apresentada neste trabalho combina um modelo a priori empirico, parâmetros neutrosféricos específicos da estação e resíduos das observações de fase GNSS. Utilizando os chamados modelos de camada única, os campos de vapor d'água atmosférico derivados são reconstruídos e visualizados, ambos em duas dimensões. Utilizando este modelo neutrosférico aumentado na geração de campos de vapor d'água dentro de uma rede regional GNSS, os resultados indicam uma melhora tanto na resolução temporal quanto na espacial dos campos de vapor d'água determinados, quando comparados com a modelagem neutrosférica convencional.

Palavras-chave: GNSS; Resíduos; Modelagem Neutrosférica; Vapor D'água Atmosférico.

1. INTRODUCTION

Although, the fraction of atmospheric water vapour in the total air mass is small, it is an environmentally significant constituent of the Earth's atmosphere. Atmospheric water vapour plays a key role in weather and climate. This gaseous water is considered to be the most important contributor (nearly 60% (MAHLBERG 2002)) to the natural green house effect which warms up the planet's surface. Just a rise of 1% of atmospheric water vapour could raise the global average temperature of Earth's surface more than 4°C (PHYSORG 2006). Therefore, quantifying the atmospheric water vapour in the global warming process is of paramount importance. Additionally, the atmospheric water vapour is inhomogeneously distributed and highly variable, which induces difficulties in determining its distribution in practice using meteorological standard sensors such as radiosonde or water vapour radiometer. The lack of detailed knowledge of the temporal variation and spatial distribution of the atmospheric water vapour is a major limiting factor towards a more accurate weather forecasting and a better understanding of the Earth's climate system.

Under the assumption that the neutrospheric effects on satellite signals, particularly introduced by atmospheric water vapour, are modelled appropriately, global satellite navigation systems (GNSS) such as GPS, GLONASS and GALILEO offer promising possibilities and cost-efficient approaches to determine atmospheric water vapour at similar quality level compared with meteorological

standard sensors. In addition, global and regional permanent GNSS networks, for example, IGS (International GNSS Service), EPN (EUREF (EUropean REference Frame) Permanent Network) and SA*POS*® (SAtellite *POSitioning Service* of the German State Survey), providing GNSS data with high temporal and spatial resolution, are capable to overcome the deficiencies of meteorological standard sensors (e.g. cost-consuming, low resolution).

Nearly 15 years ago, the determination of highly variable atmospheric water vapour based on satellite geodetic observations was realised in practice and considered as an efficient alternative to meteorological standard sensors. Various experiments have proved the good quality of this atmospheric parameter derived from GPS measurements (BEVIS ET AL. 1992, ROCKEN ET AL. 1995, 1997). The integration of GPS-based water vapour data into numerical weather models has shown significant improvement in model prediction of rainfall (GUO ET AL. 2000).

In this paper, an extended neutrospheric model for the GNSS-based determination of high-resolution atmospheric water vapour fields is presented. In Sect. 2, the three components of the extended neutrospheric model, namely empirical neutrospheric a priori model, site-specific neutrosphere parameters and residuals of GNSS phase observations are described in detail. After that, these three parts are combined to and two terms quantifying atmospheric water vapour content, namely integrated precipitable water and slant water are introduced. Sect. 3 represents an approach to reconstruct and visualise water vapour fields within a regional GNSS network by applying a planar single-layer model of the neutrosphere, whereas the visualisation results by means of the conventional and the extended neutrospheric model are compared. Conclusions and outlook follow in Sect. 4.

2. DETERMINATION OF ATMOSPHERIC WATER VAPOUR USING EXTENDED NEUTROSPHERIC MODELLING

Based on the degree of ionisation the Earth's atmosphere can be divided into the ionosphere and the neutrosphere. The electrically neutral atmosphere extends from the Earth's surface up to about 80 km and subsumes the troposphere, the stratosphere and parts of the mesosphere. The GNSS signals propagating in the neutrosphere are affected by signal delay, signal diffraction and decrease of signal power due to its non-vacuum nature. Among these three effects, the signal delay which can be represented both in time and in metric units plays the dominant role in precise positioning. In the zenithal direction, the neutrospheric delay at sea level is about 7.7 ns, or nearly 2.3 m, and it increases to more than 10 m for elevation angles of about 10°. Signal diffraction occurs whenever the direct line-of-sight between the transmitting GNSS satellite and the receiving antenna is obstructed but the GNSS signal is not completely masked. Bushes or trees are common sources for signal diffraction. This effect can be reduced by applying a realistic observation weighting model within GNSS data processing, for example, based on signal-to-

noise power ratio measurements (BRUNNER ET AL. 1999). In this case study signal diffraction is not taken into account. The decrease of signal power is caused by signal damping due to atmospheric absorption which results in a complete or partial transformation of signal power into heat.

According to HOPFIELD ET AL. (1969) the neutrospheric delay can be split into a dry and a complementary wet component. The dry delay term amounts to approx. 90% of the total neutrospheric delay and can be determined depending on air density based on the functional model described by DAVIS ET AL. (1985). Assuming that the hydrostatic equilibrium condition is valid, the air density can be easily estimated using ground pressure measurements. Consequently, the neutrospheric dry delay can be computed indirectly using ground pressure measurements. In contrast to the dry component, the complementary wet component is very difficult to handle due to high temporal and spatial variability of atmospheric water vapour. However, in order to reconstruct high-resolution atmospheric water vapour fields, the neutrospheric wet delay term must be accurately determined.

The neutrospheric wet delay can be subdivided azimuthally into an isotropic and an anisotropic part. Assuming that the atmosphere is stratified and azimuthally isotropic above a GNSS site, the wet delay term in zenith direction is conventionally determined based on an empirical neutrospheric a priori model added with the wet part of the site-specific neutrosphere parameters resulting from GNSS data processing. The anisotropic part of the wet delay existing in remaining modelling errors can be extracted from the residuals of GNSS phase observations. After scaling the isotropic component to a specific satellite elevation angle by means of a so-called mapping function, the total neutrospheric wet delay along the line-of-sight between a GNSS receiver and a satellite can be obtained.

2.1 Empirical neutrospheric a priori model

Using empirical neutrospheric a priori models (e.g. Saastamoinen model (SAASTAMOINEN 1973)), the model value of the neutrospheric zenith dry resp. wet delay $\Delta\rho_{d,0}$ resp. $\Delta\rho_{w,0}$ can be calculated depending on site-related meteorological parameters such as air temperature T [K], air pressure p [hPa] and partial pressure of water vapour e [hPa]:

$$\Delta\rho_{d,0} = 0.002277\,D\left(p - 0.155471e\right) \tag{1}$$

$$\Delta\rho_{w,0} = 0.002277\,D\left(\frac{1255}{T} + 0.205471\right)e\,, \tag{2}$$

where the factor D takes the variation of the mean gravity in the neutrospheric air column above the site into account. According to SAASTAMOINEN (1973) D can be computed depending on site latitude φ and altitude h [km] using

$$D = 1 + 0.0026\cos(2\varphi) + 0.00028h\ . \tag{3}$$

Based on surface air temperature T and relative humidity rh [%] the partial pressure of water vapour on ground can be computed, for example in the Bernese GPS Software 5.0 (BS5) (DACH ET AL. 2007) by means of

$$e = \left(\frac{rh}{100}\right) \mathrm{e}^{-37.2465 + 0.2131665 \cdot T - 0.000256908 \cdot T^2}\ , \tag{4}$$

where e denotes the Euler's number. The resulting partial pressure of water vapour using Eq. (4) does not differ significantly from the alternative meteorological models presented in GIACOMO (1982) and DAVIS ET AL. (1993). The ground meteorological parameters T, p and rh can be measured using additional meteorological sensors near the GNSS site. However, if neither measured nor representative meteorological parameters are available the standard atmosphere (ESSA/NASA/USAF 1966) related for example to mean sea level (h_0 = 0 km) with T_0, p_0 and rh_0 can be utilised, see Eq. (5)

$$\begin{aligned} T_0 &= 291.15\ \mathrm{K} \\ p_0 &= 1013.2\ \mathrm{hPa} \\ rh_0 &= 50\%. \end{aligned} \tag{5}$$

The standard atmosphere provides long-periodic information about the structure and physical properties of the Earth's atmosphere. For an arbitrary site S with altitude h_S [km] the site-related meteorological parameters T_S [K], p_S [hPa] and rh_S [%] can be extrapolated by means of formulas given in BERG (1948)

$$\begin{aligned} T_S &= T_0 - 6.5(h_S - h_0) \\ p_S &= p_0\left[1 - 0.0226(h_S - h_0)\right]^{5.225} \\ rh_S &= rh_0 \mathrm{e}^{-0.6396(h_S - h_0)}. \end{aligned} \tag{6}$$

However, due to high temporal and spatial variability of atmospheric water vapour, the wet part of the neutrospheric delay cannot be calculated sufficiently using standard empirical neutrospheric a priori models like the Saastamoinen model.

2.2 Site-specific neutrosphere parameters

In addition to an empirical neutrospheric a priori model which merely approximately describes the neutrospheric behaviour, the so-called site-specific neutrosphere parameters (SSNP) are estimated based on static GNSS observation data using scientific software like the BS5. These parameters are site- and time-

dependent zenithal corrections to the calculated a priori model values (Eq. (1) and (2)). SSNP are normally modelled in a piece-wise linear continuous way with respect to time. Assuming that the estimated SSNP represent the corrections to the total neutrospheric delay and the proportion between the wet and dry components is identical in the a priori model values and the estimated SSNP, the zenithal correction to the partial neutrospheric wet delay $SSNP_{w,0}$ can be extracted form the total *SSNP* using Eq. (7).

$$SSNP_{w,0} = SSNP \cdot \frac{\Delta\rho_{w,0}}{\Delta\rho_{d,0} + \Delta\rho_{w,0}} \tag{7}$$

Additionally, the BS5 offers the possibility to estimate horizontal neutrospheric gradient parameters which comply with the fact that the direction to the so-called neutrospheric zenith (i.e. the direction with minimum neutrospheric delay) might not be identical with the direction to the local true (or ellipsoidal) zenith. This tilting of the zenith direction is due to azimuthal asymmetries or non-parallel layering of the atmosphere and is not considered in this case study, in particular because a reliable estimation of the gradient parameters requires the use of low elevation data (e.g. below 10°) (CHEN AND HERRING 1997). Detailed information about modelling and estimation of SSNP as well as horizontal neutrospheric gradient parameters in the BS5 is given in DACH ET AL. (2007).

2.3 Anisotropic neutrospheric wet delay from GNSS residuals

High precision GNSS applications commonly use double differencing techniques to eliminate satellite and receiver clock errors as well as to reduce atmospheric effects, especially for short baselines. After the adjustment of the unknown parameters based on least-squares methods, double difference residuals (*DDR*) are obtained which contain random and remaining modelling errors. However, since the *DDR* include observations along 4 different paths (from two observation sites to two satellites), they are more difficult to interpret than single path residuals (zero difference residuals). In order to derive the information related to each single path, the conversion technique described in ALBER ET AL. (2000) is applied within this case study. It must be noted that the residuals derived from *DDR* using this technique do not necessarily correspond to the residuals of the original GNSS phase observations, because the common part of the observation errors is eliminated in the differencing process and cannot be reconstructed. Therefore, residuals derived from *DDR* are denoted as "pseudo" residuals.

Under the so-called "zero mean" assumption *DDR* can be epoch-wise converted into *PZDR* (pseudo zero difference residual) in two steps. The conversion from *DDR* to *PSDR* (pseudo single difference residual) is based on all available satellites observed at one specific epoch for an individual baseline. The conversion principle is schematically shown in Fig. 1.

Fig. 1: Conversion principle from *DDR* to *PSDR*

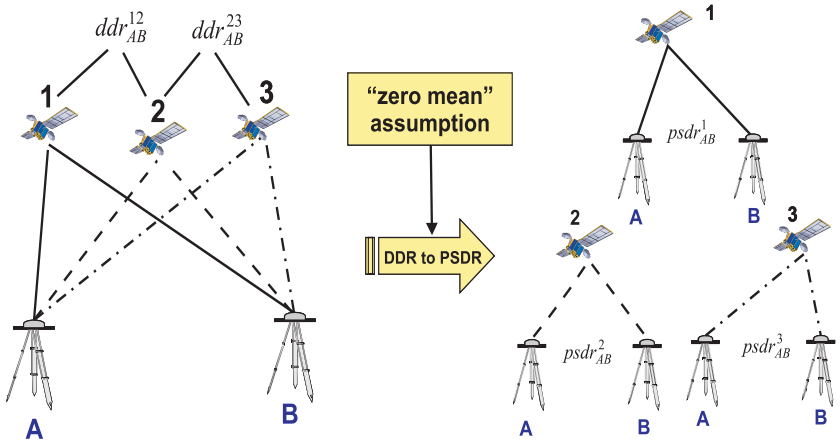

The basic mathematical relation between *DDR* and *PSDR* as well as the corresponding "zero mean" assumption for *PSDR* can be expressed in matrix form as

$$\underbrace{\begin{bmatrix} \sum_{i=1}^{n} w^i \, psdr_{AB}^i = 0 \\ ddr_{AB}^{12} \\ ddr_{AB}^{23} \\ \vdots \\ ddr_{AB}^{n-1,n} \end{bmatrix}}_{DDR} = \underbrace{\begin{bmatrix} w^1 & w^2 & w^3 & \cdots & w^n \\ 1 & -1 & 0 & \cdots & 0 \\ 0 & 1 & -1 & \cdots & 0 \\ \vdots & \vdots & \vdots & \vdots & \vdots \\ 0 & 0 & 0 & \cdots & -1 \end{bmatrix}}_{D_1} \cdot \underbrace{\begin{bmatrix} psdr_{AB}^1 \\ psdr_{AB}^2 \\ psdr_{AB}^3 \\ \vdots \\ psdr_{AB}^n \end{bmatrix}}_{PSDR} . \tag{8}$$

The "zero mean" assumption is introduced as an additional independent constraint, so that the matrix D_1 has a well-defined inverse. In order to be consistent with the weighting scheme implemented in the BS5, the elevation-dependent weight w^i

$$w^i = \sin^2 E_{AB}^i \tag{9}$$

is used, where E^i_{AB} denotes the mean value of elevation angles E^i_A and E^i_B of an individual satellite *i* related to the sites A and B. The "zero mean" postulate for *PSDR* implies that the observations must be sufficiently well modelled so that for each baseline considered in the solution, the sum of the unmodelled components of

the single difference observations is equal to zero. The "zero mean" assumption is incorrect when station biases are left in the solution (e.g. incorrect ambiguity resolution).

The subsequent conversion from *PSDR* to *PZDR* is based on all available sites within one specific epoch for an individual satellite, see Fig. 2. In this step one site must be defined as reference site.

Fig. 2: Conversion principle from *PSDR* to *PZDR*

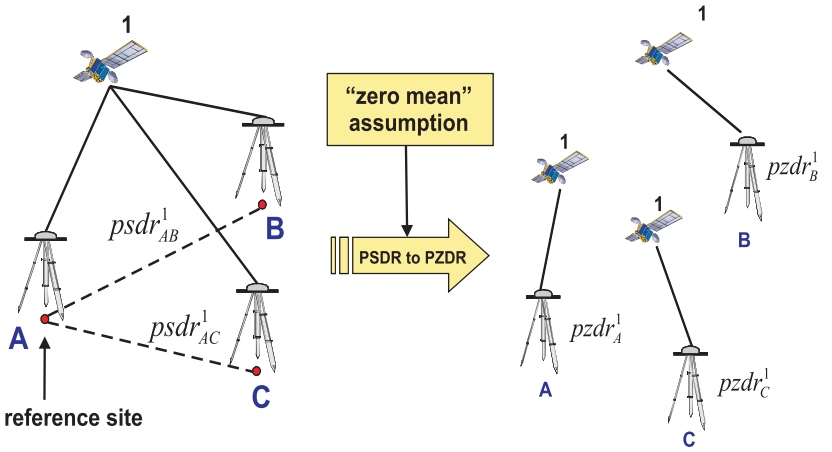

Analogously to Eq. (8), the mathematical relation between *PSDR* and *PZDR* and the corresponding "zero mean" assumption for *PZDR* can be written in matrix form as

$$\underbrace{\begin{bmatrix} \sum_{I=A}^{Z} w_I^i \, pzdr_I^i = 0 \\ psdr_{AB}^i \\ psdr_{AC}^i \\ \vdots \\ psdr_{AZ}^i \end{bmatrix}}_{PSDR} = \underbrace{\begin{bmatrix} w_A^i & w_B^i & w_C^i & \cdots & w_Z^i \\ 1 & -1 & 0 & \cdots & 0 \\ 1 & 0 & -1 & \cdots & 0 \\ \vdots & \vdots & \vdots & \vdots & \vdots \\ 1 & 0 & 0 & \cdots & -1 \end{bmatrix}}_{D_2} \cdot \underbrace{\begin{bmatrix} pzdr_A^i \\ pzdr_B^i \\ pzdr_C^i \\ \vdots \\ pzdr_Z^i \end{bmatrix}}_{PZDR}, \tag{10}$$

where the weights w^i_I can be directly calculated based on the elevation angle E^i_I of an individual satellite i related to site I. Errors in this "zero mean" assumption and the associated effects on the *PZDR* can be reduced by increasing the number of simultaneously processed network sites. Apart from the anisotropic component of the neutrospheric wet delay, the *PZDR* may contain other modelling errors due to multipath effects and phase centre variations (PCV) which are not considered in this

case study. Thus, the anisotropic wet delay derived from the *PZDR* represents the maximum-case scenario.

According to ALBER ET AL. (2000), for a GNSS network distributed over a large area (~100 km), the "zero mean" assumptions are generally valid because the distribution of atmospheric water vapour at the sites can be considered as random. Based on simulated data sets, ELOSEGUI AND DAVIS (2003) investigated this conversion strategy from a critical point of view. Using data sets from the German SA*POS*® network (SA*POS*® 2006), the numerical stability of the design matrixes D_1 (Eq. (8)) and D_2 (Eq. (10)) is analysed in LUO ET AL. (2007a).

2.4 Total neutrospheric wet delay

The computed neutrospheric a priori wet delay $\Delta\rho_{w,0}$ (Eq. (2)) and the estimated correction term $SSNP_{w,0}$ (Eq. (7)) are related to the zenith direction, while the anisotropic component $pzdr^i_I$ derived from *DDR* of GNSS phase observations is related to the line-of-sight between satellite i and receiver I. Using a so-called mapping function (*MF*), $\Delta\rho_{w,0}$ and $SSNP_{w,0}$ can be scaled to a specific satellite elevation angle E^i_I, and $pzdr^i_I$ can be conversely mapped into the zenith direction. In this case study, the wet Niell mapping function $MF_{Niell,w}$ is used with the corresponding model parameters A, B, C for the wet component of the neutrospheric delay (NIELL 1996), see Eq. (11).

$$MF_{Niell,w}(E^i_I) = \frac{1+\dfrac{A}{1+\dfrac{B}{1+C}}}{\sin E^i_I + \dfrac{A}{\sin E^i_I + \dfrac{B}{\sin E^i_I + C}}} \tag{11}$$

Based on the empirical neutrospheric a priori model $\Delta\rho_{w,0}$, the extracted neutrosphere parameter $SSNP_{w,0}$ and the converted pseudo residual $pzdr^i_I$ as well as the mapping function $MF_{Niell,w}$, the slant wet delay between satellite i and site I (SWD^i_I) can be expressed as

$$SWD^i_I = \underbrace{\underbrace{\Delta\rho_{w,0}\cdot MF_{Niell,w}}_{\text{empirical a priori model}} + \underbrace{SSNP_{w,0}\cdot MF_{Niell,w}}_{\text{neutrospheric parameter}}}_{\text{azimuthally isotropic}} + \underbrace{pzdr^i_I}_{\text{pseudo residual}}_{\text{azimutally anisotropic}} . \tag{12}$$

The corresponding zenith wet delay (ZWD^i_I) which takes the satellite-related azimuthal anisotropic component into account can be written in the form

$$ZWD_I^i = \underbrace{\underbrace{\Delta\rho_{w,0}}_{\text{empirical a priori model}} + \underbrace{SSNP_{w,0}}_{\text{neutrospheric parameter}}}_{\text{azimuthally isotropic}} + \underbrace{pzdr_I^i / MF_{Niell,w}}_{\text{pseudo residual}}}_{\text{azimuthally anisotropic}} . \tag{13}$$

The wet delay terms obtained using Eq. (12) and Eq. (13) can be translated into corresponding equivalent water vapour content. In meteorology, atmosphere scientists often relate the amount of integrated atmospheric water vapour in the zenith direction to the length [mm] of an equivalent column of liquid water which is also called integrated precipitable water (*IPW*). The ratio of *IPW* to *ZWD* defined in Eq. (14), the dimensionless factor Π, can be estimated as a function of density of liquid water ρ_w [kg/m^3], empirical constants related to the refractivity of humid air (k_3 [K^2/hPa] and $k_2^{'}$ [K/hPa]), the gas constant for water vapour (R_v [J/kgK]), and the mean temperature of the atmosphere T_m [K] using

$$\Pi = \frac{IPW}{ZWD} = 10^6 \left[\rho_w R_v \left(k_3 / T_m + k_2^{'}\right)\right]^{-1} . \tag{14}$$

According to BEVIS ET AL. (1992), T_m is highly correlated with the surface temperature T_s and therefore can be computed as follows

$$T_m = 70.2 + 0.72 \cdot T_s . \tag{15}$$

Eq. (15) is obtained based on an analysis of radiosonde data collected from stations within the United States of America and should be accurate to approx. 2% for all weather conditions. The typical value of Π is about 0.15, implying that 1 mm of *IPW* corresponds to a *ZWD* of approx. 6.5 mm. The actual value of Π varies by as much as 20% ranging from 0.12 to 0.18 depending on location, altitude, season and weather. The best possible accuracy in the estimation of *IPW* from the computed *ZWD* can be achieved if the factor Π in Eq. (14) is estimated using a value of T_m that is derived for the specific area and season. The product of *SWD* defined in Eq. (12) with Π is known as slant water (*SW*) which represents the integrated amount of precipitable water along the line-of-sight between a GNSS receiver and a satellite. *SW* provides information about the spatial distribution of atmospheric water vapour and thus holds the potential to reconstruct the three-dimensional water vapour fields after being successfully integrated into numerical weather models (MACDONALD AND XIE 2000). Other applications of *SW* measurements are related to the calibration of interferometer synthetic aperture radar (InSAR) images (HANSSEN ET AL. 1999) and tomographic modelling techniques (TROLLER 2004).

To summarise the extended neutrospheric model, Fig. 3 gives a schematic overview of the atmospheric delay effects on GNSS signals and the corresponding handling resp. modelling.

Fig. 3: Atmospheric delay effects on GNSS signals and their modelling.

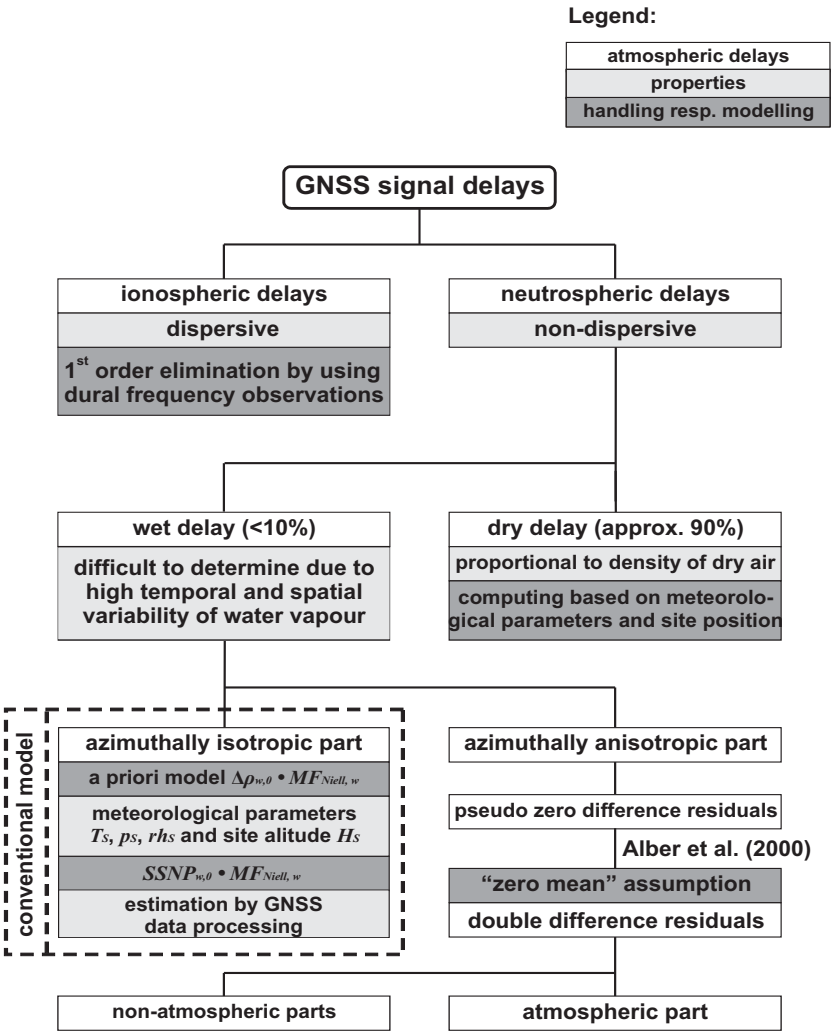

3. VISUALISATION OF ATMOSPHERIC WATER VAPOUR

In this section, based on observation data from a regional GNSS network, an approach to reconstruct and visualise atmospheric water vapour fields is presented.

After a brief description of the GNSS data base and processing strategies used in this case study, the extended neutrospheric model described in Sect. 2 is put into practice. Finally, applying a single-layer model of the neutrosphere, the determined high-resolution atmospheric water vapour fields are two-dimensionally visualised.

3.1 GNSS data base

The observation data from all sixteen sites of the SA*POS*® (Satellite *Positioning Service* of the German State Survey) network in Baden-Württemberg (Southwest Germany) covering eight days (DOY2004: 186-193) are considered within the GNSS data processing. Based on the multipath impact (MAYER ET AL. 2004), the sites are classified in three groups, see Fig. 4. For this case study the consideration of the multipath situation of the sites is meaningful, because the quasi-periodic multipath error directly affects the positioning quality. Due to the strong correlation between the neutrospheric modelling and the estimated site altitude (BEUTLER 1998), inaccurate site coordinates will inevitably produce unreliable neutrosphere parameters. Considering the weak multipath impact and the advantageous central location concerning the resulting baseline lengths, TUEB was chosen as reference site for the GNSS data processing from which fifteen baselines were formed to all other SA*POS*® sites. In Tab. 1 the most important parameter settings of the data processing are listed.

Fig. 4: SA*POS*® sites of Baden-Württemberg; multipath impact according to MAYER ET AL. (2004).

Tab. 1: Important parameter settings of the GNSS data processing using the BS5

Parameter	Characteristic
Observations Sampling rate Observation weighting model Elevation cut-off angle	GPS phase observations; double differences 180 seconds $\sin^2 E$ 10°
Orbits and earth rotation parameters	Precise final IGS products
Neutrospheric a priori model Mapping function Time span of SSNP	Model Niell $MF_{Niell,\,w}$ 2 hours
Ambiguity resolution strategy	SIGMA strategy (L5, L3)
Antenna calibration	Individual absolute calibration

3.2 Extended neutrospheric modelling

Due to the incomplete availability of meteorological data within the SA*POS*® network, the site-related meteorological parameters needed for the neutrospheric a priori model are extrapolated based on the standard atmosphere, see Eq. (5) and (6). The Saastamoinen model is used to determine the zenith neutrospheric delay terms (Eq. (1) and (2)) and the dry delay term is scaled by means of the dry Niell mapping function. For each site the a priori model values are constant over the whole observation period. The SSNP considered as corrections to the a priori model values are estimated baseline-wise with a parameter interval of 2 hours. Therefore, assuming that continuous observations are available on all sixteen SA*POS*® sites, for the reference site TUEB fifteen (depending on number of formed baselines) SSNP are estimated for each time interval of 2 h. In order to find one representative SSNP for TUEB within each time interval, the influences of the factors impacting SSNP standard deviation were analysed in LUO ET AL. (2007b). The results indicate that for long observation periods, baseline length plays the dominant role in comparison to other analysed factors. Thus, the arithmetic mean value of all SSNP estimated for TUEB within each time interval seemed to be appropriate.

In addition, the azimuthally anisotropic wet delay term in form of *PZDR* is available for each epoch (180 s), while the SSNP have a temporal resolution of 2 h. In order to derive atmospheric water vapour fields with high temporal resolution piece-wise constant SSNP are replaced by a continuous function; for this purpose the estimated SSNP values are attributed to the centres of the respective intervals (e.g. 1, 3, 5 o'clock) and considered as interpolation points. Using GNSS data over 24 h without observation gap, 24/2 + 1 = 13 parameters are estimated per site, based on piece-wise linear representation. Assuming that the parameter estimation of two consecutive days is independent, the SSNP can be interpolated between 1:00 and 24:00, while an extrapolation between 0:00 and 1:00 is necessary. In Fig. 5, the

linear and the spline approach to interpolate resp. extrapolate the estimated SSNP are compared.

Fig. 5: Inter- and extrapolation of the SSNP related to the centre of each time interval (2 h); left: site HLBR, DOY2004: 186, without observation gap, right: site FREI, DOY2004: 187, with observation gap.

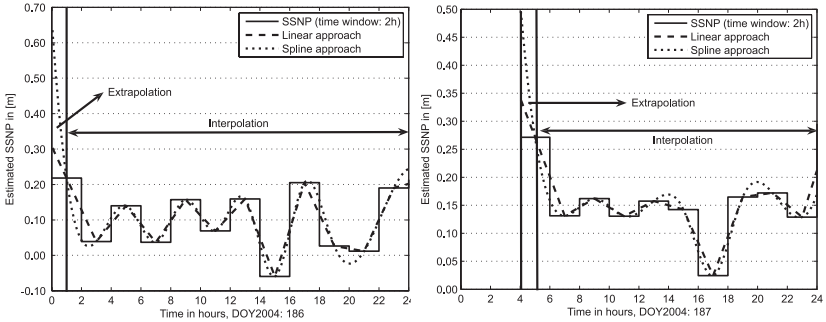

In the interpolation areas of Fig. 5 there are only marginal differences between the linear and the spline approach, while the results in extrapolation areas differ significantly and the extrapolated values using the spline approach appear to be unrealistic. Therefore, in this case study the SSNP are interpolated by means of the linear approach. It must be noted that significant differences between the consecutive SSNP values result in excessive extrapolation errors. Under these circumstances the periods where extrapolation of SSNP is necessary should not be used for generating atmospheric water vapour fields. In case of observation gaps, the corresponding SSNP cannot be estimated for the related site, as visualised between 0:00 and 4:00 in the right-hand graph of Fig. 5. Under this condition, within the affected time interval, the related site is not used for the visualisation of water vapour fields.

3.3 Atmospheric water vapour maps

Based on the extended neutrospheric model described in Sect. 2, two-dimensional water vapour fields are reconstructed and visualised by means of a so-called single-layer model. In comparison to other approaches (e.g. REIGBER ET AL. 2004) which are based on the conventional neutrospheric model and enable a routine visualisation of atmospheric water vapour fields in near real-time, the approach presented here takes the azimuthally anisotropic part into account and produces water vapour maps with high temporal and improved spatial resolution. The evaluation is carried out in the post-processing modus.

Due to the fact that 99% of the atmospheric water vapour is contained in the troposphere, a planar single-layer denoted as “water vapour map” is placed at an altitude of 10 km above mean sea level which approximately corresponds to the

altitude of the tropopause in mid-latitudes (see Fig. 6). The three-dimensional cartesian coordinates of the SA*POS*® sites (*x, y, z*) determined by GNSS data processing are transformed at first into geographic coordinates (λ, φ) and ellipsoidal heights *h*. Then the geographic coordinates are transformed into corresponding planar Gauß-Krüger coordinates using the third Gauß-Krüger zone (HECK 2003). The geoid undulation is omitted in this case study, which means that the ellipsoidal height *h* is directly used as the site altitude H_S for further calculations. Based on site coordinates and altitude, as well as on the elevation angles and azimuths of the satellites, the Gauß-Krüger coordinates of the intersection points of the GNSS signals in the water vapour map can be computed. It must be noted that the satellite azimuth is related to geographic north, but the Gauß-Krüger coordinate system refers to grid north. These north directions differ from each other due to the meridian convergence which amounts maximally to approx. 1° in this case study and must be taken into account when calculating the positions of the intersection points in the water vapour map.

For the visualisation of the determined water vapour fields, it is necessary to choose an appropriate term quantifying the water vapour content. Concerning the two terms *IPW* and *SW* introduced in Sect. 2, although *SW* provides information about the spatial distribution of atmospheric water vapour, it is not suitable for visualisation of the integrated water vapour content due to its elevation dependence. Therefore, *IPW* is used to generate water vapour maps. Taking the azimuthally anisotropic component of the neutrospheric wet delay into account, the obtained *ZWD* based on the extended neutrospheric model is related to an individual signal path, see Eq. (13). In order to obtain a 2D visualisation, the computed *IPW* representing the water vapour content along the signal path should be attributed to the centre of mass of the corresponding water vapour content. The determination of the position of the centre of mass is based on the partial pressure of water vapour *e* given in Eq. (4). In particular, the so-called full width at half maximum (FWHM) of *e* and the corresponding site-related height h_m shown in Fig. 6 are calculated.

In order to determine the centre of mass of the water vapour content along an individual signal path, the partial pressure of water vapour e_S for the site altitude H_S is firstly calculated by means of Eq. (4). The half value of e_S corresponds to the altitude H_m which is referred to mean sea level due to use of the standard atmosphere (h_0 = 0 km). The difference between H_m and H_S is the required site-related height h_m which implies the vertical position where the partial pressure of water vapour has decreased to the half of its original value e_S. h_m is site-dependent and decreases with increasing site altitude. In spite of the maximum difference of the site altitudes of nearly 620 m within the SA*POS*® network (HEID: 169.5 m, VISC: 793.5 m), the maximum difference of h_m is around 10 m (HEID: 649.6 m, VISC: 639.5m). Therefore, a constant value h_m = 650 m is used for all SA*POS*® sites to determine the projection point of the centre of mass in the water vapour map.

Fig. 6: Determination of the site-related height h_m using FWHM of water vapour pressure e; left: schematical visualisation of the principle, right: altitude dependence of e (see Eq. (4))

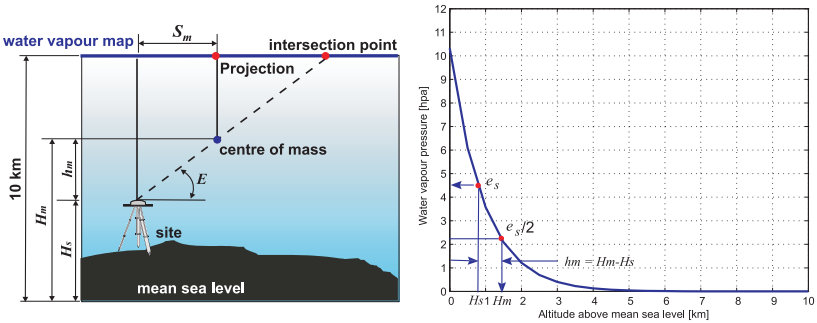

After calculating projection points of the centre of mass based on the projection length S_m (see Fig. 6, left) and reducing satellite azimuths by meridian convergence, the water vapour map can be generated by means of a two-dimensional interpolation (grid distance: 1 km) of the corresponding *IPW* values. Taking advantage of the epoch-wise derived anisotropic component, the water vapour fields can be reconstructed with high temporal resolution (minimum interval: 3 min; standard: 30 min) and with improved spatial resolution due to an increasing number of interpolation points from 16 (number of the SA*POS*® sites) to approx. 130 (number of the projection points per epoch). The water vapour maps with standard temporal resolution (30 min) are obtained by calculating the arithmetic mean of the results obtained with the maximum temporal resolution (3 min). Based on the epoch-wise generated resp. smoothed water vapour maps, animations are produced to visualise the temporal variability of the water vapour fields during the complete observation period. Fig. 7 shows an example of the generated water vapour maps with standard temporal resolution.

Since extrapolation principally is allowed for the calculation of the *IPW* values outside the boundary of the SA*POS*® network, the dashed line in Fig. 7 marks the area of the availability of the results. On DOY2004:186 the determined precipitable water vapour *IPW* varies from 7 mm to 16 mm. The magnitude of *IPW* mainly depends on the site altitude. The higher a site is situated above mean sea level, the thinner the tropospheric layer is above the site, and the lower are the corresponding *IPW* values. This can easily be validated by comparing *IPW* values at the northern sites situated in the Rhein rift (e.g. HEID) with *IPW* values at the southern sites located in the Black Forest (e.g. VISC). The minimum (min) and

maximum (max) *IPW* given additionally in Fig. 7 are related to the determined, non-interpolated values.

Fig. 7: Water vapour map (*IPW* [mm]) for the time interval 0:00-0:30, DOY2004: 186, dashed line denotes the area of availability of data.

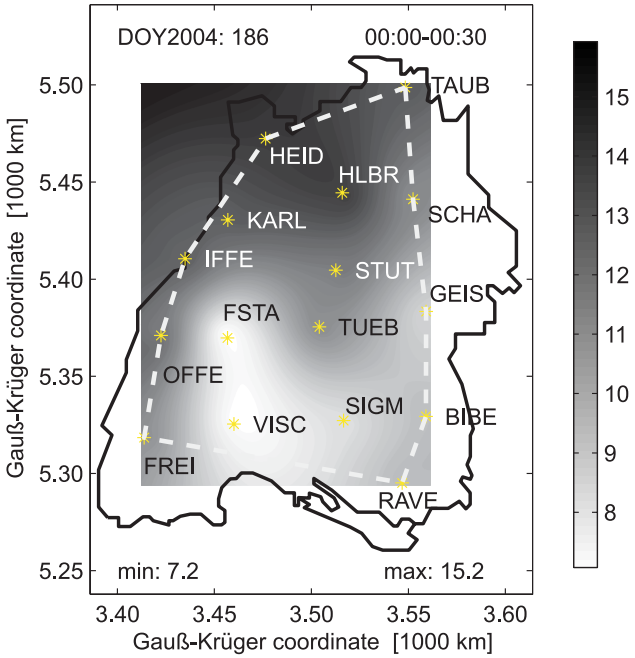

In order to demonstrate the improvements in spatial resolution, in Fig. 8 the *IPW* isolines resulting from the extended three-component neutrospheric model (M3) are compared with the corresponding results based on the conventional two-component neutrospheric model (M2) for the time interval 7:00-7:30 on DOY2004: 187. The improvements in spatial variability of atmospheric water vapour fields can be easily recognised. The conventional neutrospheric model M2 uses only the 16 SA*POS*® sites as interpolation points, while the extended neutrospheric model utilises approx. 130 satellite-related projection points coordinated in the water vapour map. On the other hand, since the conversion of *DDR* to *PZDR* is very time-consuming, it takes several hours until the final water vapour maps und animations are generated. Therefore, the extended neutrospheric model in current realisation is not suitable for real-time applications.

Fig. 8: Comparison of the isolines of *IPW*, DOY2007: 187, 7:00-7:30; left: conventional neutrospheric model (M2), right: extended neutrospheric model (M3).

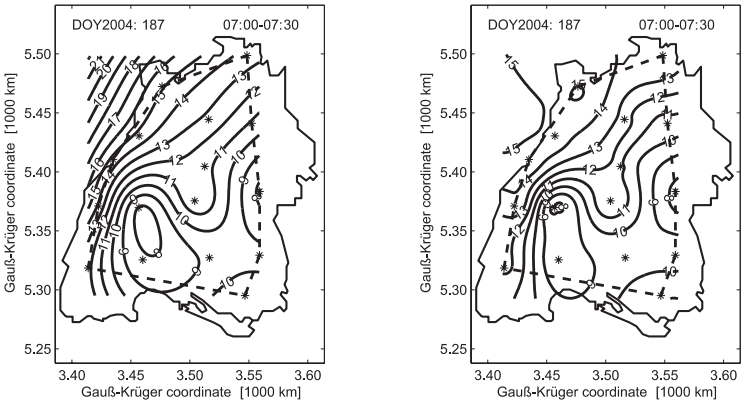

In Fig. 9, the absolute and relative differences of the determined water vapour fields using the conventional (M2) and the extended neutrospheric model (M3) are visualised for the same time interval (7:00-7:30 on DOY2004: 187). The absolute differences range between -0.4 mm and +0.8 mm and the maximum difference corresponds to approx. 10% of the mean *IPW* value. Additionally, the more significant differences are detected mainly in the southern part of the investigation area.

Fig. 9: Comparison of the conventional (M2) and the extended (M3) neutrospheric model, DOY2007: 187, 7:00-7:30; left: absolute *IPW* differences (M3-M2) [mm], right: relative *IPW* differences (|M3-M2|/M3) [%].

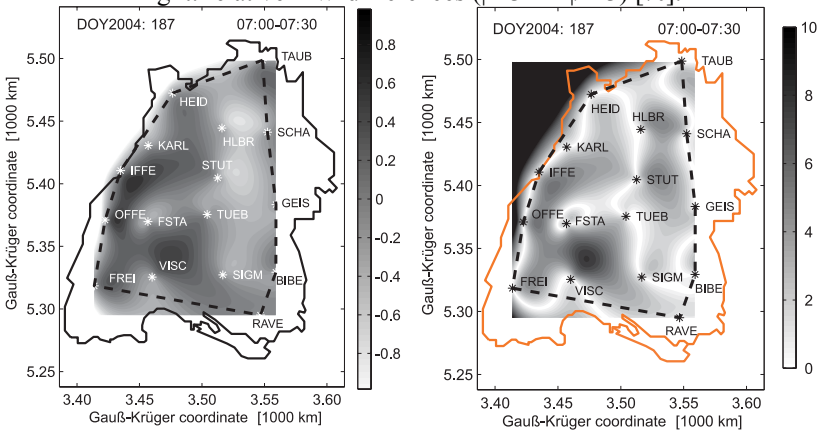

4. CONCLUSIONS AND OUTLOOK

In this paper an extended neutrospheric model, based on empirical neutrospheric a priori model, site-specific neutrosphere parameters and residuals of static GNSS phase observations, is used to determine atmospheric water vapour fields. The a priori model (here: Saastamoinen model) values of the neutrospheric delay terms are calculated under the assumption of standard atmosphere, while the site-specific neutrosphere parameters are estimated by GNSS data processing and the wet component is scaled by means of the Niell wet mapping function. After converting the double difference residuals to pseudo zero difference residuals under the "zero mean" assumption, the azimuthally anisotropic component which is usually omitted in the conventional neutrospheric model is taken into account for the calculation of the integrated precipitable water vapour content. Using GNSS data from the SA*POS*® network in Baden-Württemberg (Southwest Germany), the developed extended neutrospheric model is experimentally applied to determine atmospheric water vapour fields. Subsequently, the spatial distribution of the water vapour fields is visualised by means of a planar single-layer model. Based on the epoch-wise resp. smoothed two-dimensional water vapour maps, animations are generated to present the temporal variations of the reconstructed water vapour fields. By comparing the visualisation results, improvements both in temporal and spatial resolution of the determined water vapour fields are experienced by applying the extended neutrospheric model. These improvements with respect to the conventional neutrospheric model motivate refinements of the actual strategy for a three-dimensional determination of atmospheric water vapour fields, for example, by means of tomographic approaches.

In this case study, several simplifications and assumptions have been applied and the determination of atmospheric water vapour fields is merely based on GNSS observations. Future research work will concentrate on validation of these assumptions, refinement of the processing strategies as well as quality evaluation of the final results. The assumption that the estimated neutrosphere parameters include both the dry and the wet correction terms and the proportion of dry and wet components is identical in the neutrospheric parameters and the empirical a priori model (Eq. 7) can be validated by using ground meteorological measurements within GNSS data processing. The validation of the conversion strategy developed by ALBER ET AL. (2000) could be carried out by comparing the converted pseudo zero difference residuals (Eq. 10) with the zero difference residuals resulting from precise point positioning approaches (ZUMBERGE ET AL. 1997). In context of strategy refinement, instead of a uniform neutrosphere parameter spacing (here 2 h), a site-dependent time interval, for example, based on multipath analysis, should be investigated. Concerning the interpolation technique for the neutrosphere parameters, instead of the linear approach used in this case study, a smoothing function may be determined related to the satellite constellation. Furthermore, a

regionally optimized model (e.g. EMARDSON 1998) can be applied for the determination of the mean atmospheric temperature and its effects on the final results have to be analysed. In order to evaluate the quality of the determined water vapour content, measures provided by meteorological standard sensors such as radiosonde or water vapour radiometer can be used. After the successful realisation of these validations, modifications and evaluations, the extended neutrospheric model can be implemented into practice to determine high-resolution atmospheric water vapour fields especially for climate research.

ACKNOWLEDGEMENT

The authors would like to thank the DAAD (German Academic Exchange Service) for the financial support in the framework of the *PROBRAL* project: *Precise positioning and height determination by means of GPS: Modelling of errors and transformation into physical heights* and the department 31 of the state survey office Baden-Württemberg for providing the GNSS data and absolute antenna calibration values. Additionally, the authors gratefully acknowledge the helpful comments and valuable suggestions provided by an anonymous reviewer.

LITERATURE

ALBER, C., R.H. WARE, C.R. ROCKEN AND J. BRAUN (2000): *Obtaining single path phase delays from GPS double differences*. Geophysical Research Letters (27), pp. 2661-2664, University Corporation for Atmospheric Research (UCAR), Boulder, Colorado, USA.

BERG, H. (1948): *Allgemeine Meteorologie: Einführung in die Physik der Atmosphäre*. Dümmler Verlag, Bonn, Germany.

BEUTLER, G. (1998): *The role of GPS in space geodesy*. In: Teunissen, P.J.G., Kleusberg, A. (Eds.) GPS for geodesy. 2nd ed., Berlin, Springer Verlag, 1998, pp. 625-650.

BEVIS, M., S. BUSINGER, T.A. HERRING, C.R. ROCKEN, R.A. ANTHES AND R.H. WARE (1992): *GPS meteorology: Remote sensing of atmospheric water vapor using the Global Positioning System*. Journal of Geopysical Research (97), D14/1992, pp. 15787-15801.

BRUNNER, F.K., H. HARTINGER AND L. TROYER (1999): *GPS signal diffraction modelling: the stochastic SIGMA-Δ model*. Journal of Geodesy (73), pp. 259-267.

CHEN, G. AND T.A. HERRING (1997): *Effects of atmospheric azimuthal asymmetry on the analysis of space geodetic data*. Journal of Geophysical Research (102), B9/1997, pp. 20489-20502.

DACH, R., U. HUGENTOBLER, P. FRIDEZ AND M. MEINDL (2007): *Bernese GPS Software Version 5.0*. Astronomical Institute, University of Bern, Switzerland.

DAVIS, J.L., T.A. HERRING, I. SHAPIRO, A.E. ROGERS AND G. ELGENED (1985): *Geodesy by Interferometry: Effects of Atmospheric Modeling Errors on Estimates of Base Line Length*. Radio Science (20), 6/1985, pp. 1593-1607.

DAVIS, J.L., G. ELGERED, A.E. NIELL AND C.E. KUEHN (1993): *Ground-based measurements of gradients in the „wet" radio refractivity of air*. Radio Science (28), 6/1993, pp. 1003-1018.

ELOSEGUI, P. AND J. DAVIS (2003): *Accuracy assessment of GPS slant-path determinations*. Proceedings of the International Workshop on GPS Meteorology, Tsukuba, Japan, 14.-17. Jan. 2003 (Eds.: Iwabuchi, T. AND Shoji, Y.).

EMARDSON, T.R. (1998): *Studies of atmospheric water vapour using the Global Positioning System.* Technical Report 339, School of Electrical and Computer Engineering Charmers University of Technology, Göteborg, Sweden.

ESSA/NASA/USAF (1966): *U.S. standard atmosphere supplements, 1966*, Committee on Extension to the Standard Atmosphere, U.S. Government Printing Office, Washington, Washington D.C., USA.

GIACOMO, P. (1982): *Equation for the determination of the density of moist air (1981)*. Metrologia (18), pp. 33-40.

GUO, Y.R., Y.H. KUO, J. DUDHIA, D. PARSONS AND C.R. ROCKEN (2000): *Four-dimensional variational data assimilation of heterogeneous mesoscale observations for a strong convective case*. Monthly Weather Review (128), pp. 619-643.

HANSSEN, R., T. WECKWORTH, H. ZEBKER AND R. KLEES (1999): *High resolution water vapor mapping from interferometric radar measurements*. Science (283), pp. 1297-1299.

HECK, B. (2003): *Rechenverfahren und Auswertemodelle der Landesvermessung, Klassische und moderne Methoden*. 3nd ed.. Herbert Wichmann Verlag, Heidelberg, Germany.

HOPFIELD, H. (1969): *Two-quartic tropospheric refractivity profile for correcting satellite data*. Journal of Geophysical Research (74), 18/1969, pp. 4487-4499.

LUO, X., M. MAYER AND B. HECK (2007a): *Quantifizierung verschiedener Einflussfaktoren in GNSS-Residuen*. Zeitschrift für Geodäsie, Geoinformation und Landmanagement (ZfV) (132), pp. 97-107.

LUO, X., M. MAYER AND B. HECK (2007b): *Bestimmung von hochauflösenden Wasserdampffeldern unter Berücksichtigung von GNSS-Doppeldifferenzresiduen*. Schriftenreihe des Studiengangs Geodäsie und Geoinformatik, 2/2007, Universität Karlsruhe (TH), Karlsruhe, Germany. Link: http://www.uvka.de/univerlag/volltexte/2007/203/

MACDONALD, A. AND Y. XIE (2000): *On the use of slant observations from GPS to diagnose three dimensional water vapor using 3DVAR*. Paper presented at 4th Integrated Observing Systems Symposium, Jan., 2000. American Meteorological Society, Long Beach, California, USA.

MALBERG, H. (2002): *Meteorologie und Klimatologie*. 4nd ed., Springer-Verlag, Berlin, Germany.

MAYER, M., L. WANNINGER, H.-G. DICK, H. DERENBACH AND B., HECK (2004): *Mehrwegeeinflüsse auf den* SA*POS*®*-Stationen Baden-Württembergs*, Poster, Geodätische Woche 2004, Stuttgart 12.-15. Oktober 2004. Link: https://www.gik.uni-karlsruhe.de/fileadmin/mitarbeiter/mayer/poster_gw2004/poster_gw_2004_mp.pdf

NIELL, A.E. (1996): *Global mapping functions for the atmosphere delay at radio wavelengths*. Journal of Geophysical Research (101), B2/1996, pp. 3227-3246.

PHYSORG (2006): *Greenhouse theory smashed by biggest stone.* www.physorg.com/news11710.html, published March 14, 2006, cited August 28, 2007.

REIGBER, C., G. GENDT AND J. WICKERT (2004): *GPS Atmosphären-Sondierungs-Projekt (GASP) - Ein innovativer Ansatz zur Bestimmung von Atmosphärenparametern*. Abschlussbericht, HGF-Strategiefonds-Projekt GASP - FKZ 01SF9922 des AWI, DLR, GFZ und GKSS, Scientific Technical Report, 04/02, 2004.

ROCKEN, C.R., T. VAN HOVE, J.M. JOHNSON, F.S. SOLHEIM AND R.H. WARE (1995): *GPS/STORM: GPS sensing of atmospheric water vapor for meteorology*. Journal of Atmospheric and Oceanic Technology (12), pp. 468-478.

ROCKEN, C., T. VAN HOVE AND R. H. WARE (1997): *Near real-time GPS sensing of atmospheric water vapor*. Geophysical Research Letters (24), pp. 3221-3224.

SAASTAMOINEN, J. (1973): *Contributions to the theory of atmospheric refraction*. Bulletin Géodésique (48), pp. 279-298, (48), pp. 383-397, (49), pp. 13-34.

SA*POS*® (2006): State survey office Baden-Württemberg, Link: http://www.lv-bw.de/lvshop2 /ProduktInfo/sapos/sapos_1_adv.htm, cited May 30, 2006.

TROLLER, M. (2004): *GPS based Determination of the Integrated and Spatially Distributed Water Vapor in the Troposphere*. Geodätisch-geophysikalische Arbeiten in der Schweiz, Schweizerische Geodätische Kommission, Vol. 67, Zürich, Switzerland.

ZUMBERGE, J.F., M.B. HEFLIN, D.C. JEFFERSON AND M.M. WATKINS (1997): *Precise point positioning for the efficient and robust analysis of GPS data from large networks*. Journal of Geophysical Research (102), pp. 5005-5017.

(Recebido em fevereiro/08. Aceito em maio/08)